Annals of Nuclear Energy 175 (2022) 109246

Contents lists available at ScienceDirect

Annals of Nuclear Energy

journal homepage: www.elsevier.com/locate/anucene

Edge-wise perturbations to model vibrating fuel assemblies in the frequency-domain using FEMFFUSION: Development and verification

A. Vidal-Ferràndiz [b,*], A. Carreño [a], D. Ginestar [b], G. Verdú [a]

[a] Instituto Universitario de Matemática Multidisciplinar, Universitat Politècnica de València, Camáde Vera s/n, 46022 València, Spain
[b] Instituto de Seguridad Industrial: Radiofísica y Medioambiental, Universitat Politècnica de València, Camáde Vera s/n, 46022 València, Spain

ARTICLE INFO

Article history:
Received 28 January 2022
Received in revised form 24 April 2022
Accepted 25 May 2022
Available online 2 June 2022

Keywords:
Neutron noise
Fuel assembly vibrations
Neutron diffusion
Frequency domain
Noise analysis

ABSTRACT

The mechanical vibrations of fuel assemblies have shown to give high levels of neutron noise, triggering in some circumstances the necessity to operate nuclear reactors at a reduced power level. This behaviour can be modelled using the neutron noise diffusion approximation in the frequency-domain. This work presents an extension of the finite element method code FEMFFUSION, to simulate mechanical vibrations in hexagonal reactors in the frequency domain. This novel strategy in neutron noise simulation is based on introducing perturbations on the edges of the cells associated with the vibrating fuel assemblies, allowing to model the movement of these fuel assemblies accurately and efficiently, without the necessity of using locally refined meshes. Numerical results verify the edge-wise methodology in the frequency-domain against the usual cell-wise frequency-domain model and the time-domain model. The edge-wise frequency-domain methodology has also been compared to other neutronic codes, as CORE SIM+ and PARCS.

1. Introduction

The neutron noise is defined as the fluctuations of the neutron flux over its steady state. These oscillations in the neutron field can be caused by the statistical properties of the underlying nuclear processes of fission chains (*branching noise*) or due to small perturbations in the operation of a nuclear reactor (*power noise*). The power neutron noise can be used to detect and localize its causing anomalies. The early detection of such perturbations gives the possibility to take proper actions before they affect the plant availability and safety. One important type of anomaly in a nuclear power plant is mechanically vibrating fuel assemblies (FA). In the context of the Euratom CORTEX project Demazière et al. (2017), the effect of mechanical vibrations has been studied in depth.

One useful technique to estimate the effect of a vibrating FA in the neutron noise is to resolve the time-dependent neutron diffusion equation for this transient (Vidal-Ferràndiz et al., 2020). A numerical discrete Fourier transform is then performed to compare the obtained results with the frequency-domain analysis. The main advantage of the time-domain model is that it does not imply any approximation in the perturbations. However, it needs to solve accurately a large system of linear equations at each time-step where the change in the neutron flux is quite small.

On the other hand, the first-order frequency-domain neutron noise equation in the diffusion approximation can be solved for interesting perturbations (Demazière, 2011; Mylonakis et al., 2021). This equation must be solved after finding the steady state of the reactor, since the static neutron flux is a variable of this equation. The first-order noise equation is derived by considering the static equations associated with the time-dependent ones and assuming that the fluctuations are much smaller than the mean values to be able to neglect second-order terms. A Fourier transform is then performed to obtain a large linear system with complex values in the frequency-domain. This methodology has been applied to rectangular (Mylonakis et al., 2020; Mylonakis et al., 2021; Kolali et al., 2021) and hexagonal reactors (Malmir and Vosoughi, 2015; Hosseini et al., 2018; Hosseini and Mohamadbeygi, 2021). Moreover, better approximations of the neutron transport equation have been also applied to neutron noise simulations as Monte Carlo calculations (Rouchon et al., 2017; Yamamoto, 2018) or deterministic strategies as the method of characteristic (Gammicchia et al., 2020), the discrete ordinates approximation (Yi et al., 2021) and the SP_3 approximation (Gong et al., 2021).

Generally, to simulate the neutron noise mechanical vibrations, refined meshes around the perturbed cell assembly are required

* Corresponding author.
E-mail addresses: anvifer2@upv.es (A. Vidal-Ferràndiz), amcarsan@iqn.upv.es (A. Carreño), dginesta@mat.upv.es (D. Ginestar), gverdu@iqn.upv.es (G. Verdú).

https://doi.org/10.1016/j.anucene.2022.109246
0306-4549/

(Vidal-Ferràndiz et al., 2020), which leads to complicated geometric problems if non-rectangular grids in the spatial discretization are used. This work presents an alternative methodology to simulate the neutron noise produced by mechanical vibrations using the frequency-domain model for the diffusion approximation and the finite element method (FEM), the edge-wise strategy. This methodology permits to introduce perturbations on the edges of the cells to simulate the mechanical vibration of the fuel assemblies. The edge-wise strategy makes use of the shape functions defined on the faces of the finite element cells. This strategy is verified, for rectangular and hexagonal reactors, with the time-domain methodology presented in (Vidal-Ferràndiz et al., 2019; Vidal-Ferràndiz et al., 2020). The developed codes are an extension of the open source neutron diffusion solver `FEMFFUSION` (Vidal-Ferràndiz et al., 2021).

The rest of the manuscript is organized as follows. Section 2 describes the neutron diffusion equation in the time-domain. This Section includes a brief description of the finite element discretization. Section 3 describes the frequency-domain first-order neutron noise equation and its discretization with the finite element method. Section 4 explains different strategies to introduce a mechanical vibration perturbation in the frequency-domain in complex geometries. Section 5 compares numerically the new edge-wise frequency-domain model with the time-domain and classical frequency-domain methodologies for rectangular and hexagonal problems. Finally, the conclusions of the work are presented in Section 6.

2. Time-dependent neutron diffusion equation

The multigroup time-dependent neutron diffusion equation can be written as (Stacey, 2007),

$$\mathscr{V}\frac{\partial \Phi}{\partial t} + \mathscr{L}\Phi = (1-\beta)\mathscr{M}\Phi + \sum_{k=1}^{K}\lambda_k \mathscr{X}_k \mathscr{C}_k, \tag{1}$$

where the concentrations of the neutron precursors are given by

$$\frac{\partial \mathscr{C}_k}{\partial t} = \beta_k \mathscr{F}\Phi - \lambda_k^d \mathscr{C}_k, \qquad k = 1,\dots,K. \tag{2}$$

In the previous expressions, the matrices for G energy groups are defined as,

$$\Phi = (\,\phi_1 \quad \phi_2 \quad \cdots \quad \phi_G\,)^T, \qquad \mathscr{F} = (\,\nu\Sigma_{f1} \quad \cdots \quad \nu\Sigma_{fG}\,), \qquad \mathscr{L} = \mathscr{L}_D + \mathscr{L}_A \tag{3}$$

$$\mathscr{L}_D = \begin{pmatrix} -\vec{\nabla}\cdot\left(D_1\vec{\nabla}\right) & \dots & 0 \\ \vdots & \ddots & \vdots \\ 0 & \dots & -\vec{\nabla}\cdot\left(D_G\vec{\nabla}\right) \end{pmatrix},$$

$$\mathscr{L}_A = \begin{pmatrix} \Sigma_{a1} + \sum\limits_{g'=1,g'\neq g}^{G}\Sigma_{sgg'} & \dots & -\Sigma_{sG1} \\ \vdots & \ddots & \vdots \\ -\Sigma_{s1G} & \dots & \Sigma_{aG} + \sum\limits_{g'=1,g'\neq g}^{G}\Sigma_{sgg'} \end{pmatrix}, \tag{4}$$

$$\mathscr{M} = \begin{pmatrix} \chi_1^p\nu\Sigma_{f1} & \dots & \chi_1^p\nu\Sigma_{fG} \\ \vdots & \ddots & \vdots \\ \chi_G^p\nu\Sigma_{f1} & \dots & \chi_G^p\nu\Sigma_{fG} \end{pmatrix}, \qquad \mathscr{V} = \begin{pmatrix} 1/\mathrm{v}_1 & \dots & 0 \\ \vdots & \ddots & 0 \\ 0 & \dots & 1/\mathrm{v}_G \end{pmatrix},$$

$$\mathscr{X}_k = \begin{pmatrix} \chi_1^{d,k} \\ \vdots \\ \chi_G^{d,k} \end{pmatrix}, \tag{5}$$

where the main unknowns of the neutron diffusion equation are the space- and time-dependent neutron flux $\Phi(\vec{r},t)$ and the delayed neutron precursor concentrations $\mathscr{C}_k(\vec{r},t)$ for the k-th precursor group $k = 1,\dots,K$. The rest of magnitudes are also space and time dependent quantities that depend on the reactor materials. The diffusion coefficient for the g-th energy group is represented by D_g. The absorption and the fission macroscopic cross-sections are denoted by Σ_{ag} and Σ_{fg}, respectively. The value of $\Sigma_{sgg'}$ is the scattering cross section that goes from the g' energy group to the g energy group. The value of ν is the mean number of neutrons produced by fission. The value of v_g denotes the neutron velocity. The spectrum of the prompt and the delayed neutrons are denoted by χ_g^p and $\chi_g^{d,k}$, and in this work they are assumed equal, i.e. $\chi_g^p = \chi_g^{d,k}$ for $g = 1,\dots,G$, so we simply denote $\mathscr{X} := \mathscr{X}_k$ and then, $\mathscr{M} = \mathscr{X}\mathscr{F}$. The fraction of the delayed neutrons is β_k such that the total delayed neutron fraction $\beta = \sum_{k=1}^{K}\beta_k$. Finally, the neutron precursor delayed constants are represented by λ_k^d.

To solve the differential equations, a spatial discretization of the equations must be selected. In this work, a high order continuous Galerkin finite element method (Zienkiewicz et al., 2013) is used, leading to a time-dependent algebraic system of ordinary differential equations. The continuous Galerkin method is the most usual finite element method because it is more economical from the memory usage point of view.. In particular, Lagrange polynomials $\mathscr{N}_a(\vec{r})$ are used to approximate the neutron flux and the concentration of precursors as a sum of shape functions multiplied by the unknown expansion coefficients as

$$\Phi \approx \sum_{a=0}^{N_{\text{dofs}}}\mathscr{N}_a\tilde{\Phi}_a, \qquad \mathscr{C}_k \approx \sum_{a=0}^{N_{\text{dofs}}}\mathscr{N}_a C_{k,a}. \tag{6}$$

where N_{dofs} is the number of weights of the Lagrange polynomials used in the finite element method to model the problem, in other words, the number of degrees of freedom of the problem.

Introducing the weak formulations in Eqs. (1) and (2), and considering these resulting expansions and the Galerkin approximation yield a system of discretized equations

$$V\frac{d\tilde{\Phi}}{dt} + L\tilde{\Phi} = (1-\beta)M\tilde{\Phi} + \sum_{k=1}^{K}\lambda_k^d \mathscr{X} C_k, \tag{7}$$

$$\frac{dC_k}{dt} = \beta_k F\tilde{\Phi} - \lambda_k^d C_k, \qquad k = 1,\dots,K, \tag{8}$$

where L, M, F and V are the matrices obtained from the discretization of operators $\mathscr{L}, \mathscr{M}, \mathscr{F}$ and $\mathscr{V}$, respectively. More details can be found in (Vidal-Ferràndiz et al., 2014; Vidal-Ferràndiz et al., 2016). This finite element method has been implemented by using the open source finite elements' library `deal.ii` (Bangerth et al., 2007).

To integrate the time-dependent equation, a semi-implicit scheme of first order is applied (Vidal-Ferràndiz et al., 2016). The time interval $[0,T]$ is divided into several subintervals $[t_h, t_{h+1}]$. First, the moments at $t = t_{h+1}$ are approximated by applying a backward difference of first order for the partial time derivative. The rest of terms is then substituted by its value at time t_{h+1}, except the concentration of precursors term that is substituted by its value at time t_h. Under these assumptions, the vector of neutron flux at time t_{h+1} is approximated by solving a linear system. The concentration of precursors is updated along the time by using a backward difference of first order. The resulting algebraic linear systems are solved by using the GMRES method provided from PETSc library (Balay et al., 2021) and the block preconditioner developed in (Vidal-Ferràndiz et al., 2020).

For a given transient analysis in a reactor core, a static configuration of the reactor is necessary to be considered as initial condition. Usually, the solution of the λ-modes problem associated with the time dependent neutron diffusion equation,

$$L_0\tilde{\Phi}_0 = \frac{1}{\lambda}M_0\tilde{\Phi}_0, \tag{9}$$

where subindex 0 denotes the value of the matrix for the configuration of the core at $t = 0$, is used for this purpose (Verdú et al., 1994). The fundamental eigenvalue is called the k-effective of the reactor core, and its corresponding eigenfunction describes the steady state neutron distribution in the core. This problem is solved using the methodology presented in (Vidal-Ferràndiz et al., 2014). In this work, we start with a critical configuration of the reactor by dividing the fission cross-sections by the k-effective.

3. First-Order Neutron Noise Equation

The first-order neutron noise theory is developed by splitting every time dependent term, expressed as $X(\vec{r}, t)$, into their mean value, X_0, which is considered as the steady-state solution, and their fluctuation around the mean value, δX, as

$$X(\vec{r}, t) = X_0(\vec{r}) + \delta X(\vec{r}, t). \tag{10}$$

These fluctuations are assumed to be small compared to the mean values $|\delta X(\vec{r}, t)| \ll |X_0(\vec{r})|$. This allows to neglect second-order terms $(\delta X(\vec{r}, t) \times \delta X(\vec{r}, t)) \approx 0$.

The different magnitudes are then split as,

$$\mathscr{L} = \mathscr{L}_0 + \delta\mathscr{L} = \mathscr{L}_{D0} + \mathscr{L}_{A0} + \delta\mathscr{L}_A, \tag{11}$$

$$\mathscr{M} = \mathscr{M}_0 + \delta\mathscr{M}, \tag{12}$$

$$\mathscr{F} = \mathscr{F}_0 + \delta\mathscr{F}, \tag{13}$$

$$\Phi = \Phi_0 + \delta\Phi, \tag{14}$$

$$\mathscr{C}_k = \mathscr{C}_{k,0} + \delta\mathscr{C}_k. \tag{15}$$

where the fluctuations of the diffusion coefficients are neglected (i.e. $\delta D_g \approx 0$). Therefore, $\delta\mathscr{L} = \delta\mathscr{L}_A$. These approximations were demonstrated to be valid for light water reactor applications (Larsson and Demazière, 2009; Vidal-Ferràndiz et al., 2020). Moreover, we have assumed that the fissile element does not change during the transient, so $\delta\mathscr{X} = 0$. Neutron precursor data (β_k, λ_k^d) and velocities do not fluctuate along the time either.

Applying the neutron noise separations from (11) to (15) into Eqs. (1) and (2), removing the second-order terms, and using the static Eqs. (9), we obtain the first-order neutron noise diffusion equation,

$$\mathscr{V}\frac{\partial}{\partial t}\delta\Phi = -\mathscr{L}_0\delta\Phi - \delta\mathscr{L}_A\Phi_0 + (1-\beta)\mathscr{M}_0\delta\Phi + (1-\beta)\delta\mathscr{M}\Phi_0 + \sum_{k=1}^{K}\lambda_k^d\mathscr{X}\delta\mathscr{C}_k, \tag{16}$$

$$\frac{\partial}{\partial t}\delta\mathscr{C}_k = \beta_k\delta\mathscr{F}\Phi_0 + \beta_k\mathscr{F}_0\delta\Phi - \lambda_k^d\delta\mathscr{C}_k, \quad k = 1,\ldots,K. \tag{17}$$

After that, a Fourier Transform defined as,

$$f(\omega) = \mathscr{F}[f(t)](\omega) = \int_{-\infty}^{\infty}\exp(-i\omega t)f(t)dt, \tag{18}$$

is performed to get

$$\mathscr{V}i\omega\delta\Phi = -\mathscr{L}_0\delta\Phi - \delta\mathscr{L}_A\Phi_0 + (1-\beta)\mathscr{M}_0\delta\Phi + (1-\beta)\delta\mathscr{M}\Phi_0 + \sum_{k=1}^{K}\lambda_k^d\mathscr{X}\delta\mathscr{C}_k, \tag{19}$$

$$i\omega\delta\mathscr{C}_k = \beta_k\delta\mathscr{F}\Phi_0 + \beta_k\mathscr{F}_0\delta\Phi - \lambda_k^d\delta\mathscr{C}_k, \quad k = 1,\ldots,K. \tag{20}$$

This frequency-domain formulation permits substituting the equations related with the concentration of the delayed neutron precursors (20) into the equation of the neutron flux (19). This step leads to the multigroup neutron noise diffusion equation,

$$(i\omega\mathscr{V} + \mathscr{L}_0 - \gamma\mathscr{M}_0)\delta\Phi = (-\delta\mathscr{L} + \gamma\delta\mathscr{M})\Phi_0, \tag{21}$$

where

$$\gamma = (1-\beta) + \sum_{k=1}^{K}\frac{\lambda_k\beta_k}{i\omega + \lambda_k}. \tag{22}$$

In the usual 2 energy groups approximation and without considering up-scattering, the first-order diffusion neutron noise equation can be written as

$$\mathscr{A}\delta\Phi = \mathscr{B}\Phi_0, \tag{23}$$

where

$$\mathscr{A} = \begin{bmatrix} \frac{i\omega}{v_1} - \vec{\nabla}D_1\vec{\nabla} + \Sigma_{a1}^0 + \Sigma_{12}^0 - \gamma\nu\Sigma_{f1}^0 & -\gamma\nu\Sigma_{f2}^0 \\ -\Sigma_{12}^0 & \frac{i\omega}{v_2} - \vec{\nabla}D_2\vec{\nabla} + \Sigma_{a2} \end{bmatrix},$$
$$\mathscr{B} = \begin{bmatrix} -\delta\Sigma_{a1} - \delta\Sigma_{12} + \gamma\delta\nu\Sigma_{f1} & +\gamma\delta\nu\Sigma_{f2} \\ \delta\Sigma_{12} & -\delta\Sigma_{a2} \end{bmatrix}. \tag{24}$$

4. Cell-wise and edge-wise models of a vibrating fuel assembly

Now, we describe how to model the vibration of a FA as a perturbation of cross sections in the frequency-domain, following the "ϵ/D model", (Pázsit, 1988; Jonsson et al., 2012; Vidal-Ferràndiz et al., 2020; Zoia et al., 2021). In the following, a mechanical oscillating FA is modelled as several vibrating interfaces between homogeneous materials. The cross section, Σ_α, at the interface $x = b$ between two material regions, as the one shown in Fig. 1, is described as:

$$\Sigma_\alpha(x) = (1 - \mathscr{H}(x-b))\Sigma_\alpha^I + \mathscr{H}(x-b)\Sigma_\alpha^{II}, \tag{25}$$

where $\mathscr{H}$ is the unit step function, Σ_α^I and Σ_α^{II} are the cross sections at region I and II, respectively. Therefore, a vibrating assembly can be described as two in-phase moving interfaces (one moving interface on one side of the assembly and another moving interface on the other side of the moving assembly). For the sake of simplicity, only one moving interface is first considered in the derivations presented hereafter.

An interface moving as $b(t) = b_0 + \epsilon\sin(\omega_p t)$, results in:

$$\Sigma_\alpha(x,t) = \left(1 - \mathscr{H}(x - b_0 - \epsilon\sin(\omega_p t))\right)\Sigma_\alpha^I + \mathscr{H}(x - b_0 - \epsilon\sin(\omega_p t))\Sigma_\alpha^{II}. \tag{26}$$

Using a first order Taylor expansion, the cross section perturbation can be expressed as

$$\delta\Sigma_\alpha(x,t) = \left(\Sigma_\alpha^I - \Sigma_\alpha^{II}\right)\epsilon\sin(\omega_p t))\delta(x - b_0), \tag{27}$$

and, in the frequency-domain, the perturbation is written as follows

$$\delta\Sigma_\alpha(x,\omega) = -i\pi\epsilon\left(\Sigma_\alpha^I - \Sigma_\alpha^{II}\right)\delta(x - b_0)(\delta(\omega - \omega_p) + \delta(\omega + \omega_p)). \tag{28}$$

where the contributions associated with frequencies different to the vibrating frequency, ω_p, are neglected, including the negative frequencies. The effect of second harmonics is studied in (Zoia et al., 2021 and Vidal-Ferràndiz et al., 2020).

Now, it is assumed that in Eq. (23),

$$\delta\Phi(\vec{r}, \omega) = \delta\hat{\Phi}(\vec{r})\,\delta(\omega - \omega_p), \tag{29}$$

$$\mathscr{B}(\vec{r}, \omega) = \delta\hat{\mathscr{B}}(\vec{r})\,\delta(\omega - \omega_p). \tag{30}$$

Thus, the equation to be solved is

$$\mathscr{A}(\omega_p)\delta\hat{\Phi} = \hat{\mathscr{B}}\Phi_0, \tag{31}$$

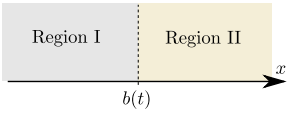

Fig. 1. Vibrating interface between two regions.

where $\mathscr{A}(\omega_p)$ is the operator $\mathscr{A}$ evaluated at $\omega = \omega_p$, so that the term $\delta(\omega - \omega_p)$ is not introduced in the numerical calculation.

For the spatial discretization of Eq. (31) it is used the same continuous Galerkin finite element method as in the one selected for the time-domain formulation of Eq. (21), obtaining, in this way, an algebraic linear system of equations with the following structure

$$A\,\delta\tilde{\Phi} = B\,\tilde{\Phi}_0, \tag{32}$$

where

$$A = (i\omega V + L_0 - \gamma M_0), \qquad B = (-\delta L + \gamma \delta M),$$

$L_0, M_0, \delta L$, δM and V are the matrices obtained from the discretization of operators $\mathscr{L}_0, \mathscr{M}_0, \delta\mathscr{L}, \delta\mathscr{M}$ and $\mathscr{V}$, respectively. The unknowns vector $\delta\tilde{\Phi}$ contains the corresponding coefficients of $\delta\Phi$ in terms of the Lagrange polynomials. The vector $\tilde{\Phi}_0$ is the discretization of the static neutron flux, which is obtained from the solution of the λ-modes problem (9). The spatial discretization for the static problem and the neutron noise problem must be the same in order to get coherent results because the reactor must be critical before the frequency-domain calculation is undertaken.

To treat the term $\delta(x - b_0)$, appearing in Eq. (28) in the spatial discretization,we can make use of the conventional cell-wise methodology or the novel edge-wise one.

4.1. Cell-Wise Methodology

A common approximation consists of distributing the cross section perturbation over the spatial region of the vibration, *cell-wise* methodology (CW), which is convenient for cell-based codes (Demazière, 2011; Vidal-Ferràndiz et al., 2020). This approximation is based on the fact that, for a small ϵ, the delta distribution can be approximated by a suitable nascent delta function, F_ϵ,

$$\delta(x) \simeq F_\epsilon = \begin{cases} \frac{1}{2\epsilon} & x \in [-\epsilon, +\epsilon] \\ 0 & x\text{otherwise} \end{cases} \tag{33}$$

so that ϵ at the denominator cancels out with the term of the first-order contribution in the Taylor expansion.

$$\delta\Sigma_\alpha^{(CW)}(x) = -\frac{i\pi}{2}\left(\Sigma_\alpha^{I} - \Sigma_\alpha^{II}\right), \quad x \in [-\epsilon, +\epsilon]. \tag{34}$$

To introduce this perturbation in the finite element calculation, the matrix B is given by:

$$B = \begin{bmatrix} B_{11} & \cdots & B_{G1} \\ \vdots & \ddots & \vdots \\ B_{G1} & \cdots & B_{GG} \end{bmatrix}, \tag{35}$$

where the element ij of the block gh is given by:

$$B_{gh}(i,j) = \sum_{e=1}^{N_e} \mathscr{B}_{gh}^{(e)} \int_{\Omega_e} \mathscr{N}_i \mathscr{N}_j dV, \tag{36}$$

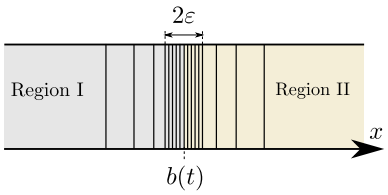

Fig. 2. Example of a locally refined mesh around the interface perturbation for a cell-wise methodology.

where the perturbed area Ω have been divided into N_e elements, such that $\Omega = \bigcup_{e=1}^{N_e} \Omega_e$. $\mathscr{B}_{gh}^{(e)}$ is the value of $\mathscr{B}_{gh}$ at the cell e using the cell-wise perturbed cross sections defined in Eq. (34).

To obtain an accurate solution of the neutron noise with the cell-wise methodology, it is necessary to use locally refined meshes around the interface perturbation, as the one shown in Fig. 2. This local refinement produces numerous cells and, thus, bigger matrices associated with the linear systems need to be solved. Also, take into account that to construct this refined mesh compatible with the hexagonal geometry is a difficult task that has to be constructed specifically for each perturbed assembly. This type of refined meshes can contain hanging nodes or unstructured zones.

4.2. Edge-wise methodology

Another possibility is to directly introduce the perturbation on the edges of the vibrating assembly, *edge-wise* methodology (EW). Using this strategy, the use of a refined mesh near the perturbation is avoided. The perturbation is

$$\delta\Sigma_\alpha^{(EW)}(x) = -i\pi\epsilon\left(\Sigma_\alpha^{I} - \Sigma_\alpha^{II}\right), \quad x \in \Gamma_f, \tag{37}$$

where Γ_f is a fuel assembly edge where the perturbation is introduced. This scheme can be implemented in the finite element method through the integrals along the perturbed edges,

$$B_{gh}(i,j) = \sum_{f=1}^{N_f} \mathscr{B}_{gh}^{(f)} \int_{\Gamma_f} \mathscr{N}_i \mathscr{N}_j dS, \tag{38}$$

where $\mathscr{B}_{gh}^{(f)}$ is the value of $\mathscr{B}_{gh}$ at the face f using the edge-wise perturbed cross sections defined in Eq. (37). This integral over the edge of the cell appears also in the treatment of vacuum and albedo boundary conditions when the high-order finite element method is used, (Vidal-Ferràndiz et al., 2014; González-Pintor et al., 2009).

This edge-wise strategy permits to efficiently introduce mechanical FA vibrations in hexagonal reactors. Fig. 3 shows a vibration in the x direction and the edge-wise calculation can be written as:

$$\delta\Sigma_\alpha^{EW(a)} = i\pi\epsilon\cos(\pi/3)\left(\Sigma_\alpha^{(1)} - \Sigma_\alpha^{(4)}\right) = \frac{i\pi\epsilon}{2}\left(\Sigma_\alpha^{(1)} - \Sigma_\alpha^{(4)}\right), \tag{39}$$

$$\delta\Sigma_\alpha^{EW(b)} = i\pi\epsilon\cos(\pi/3)\left(\Sigma_\alpha^{(4)} - \Sigma_\alpha^{(2)}\right) = \frac{i\pi\epsilon}{2}\left(\Sigma_\alpha^{(4)} - \Sigma_\alpha^{(2)}\right), \tag{40}$$

$$\delta\Sigma_\alpha^{EW(c)} = i\pi\epsilon\left(\Sigma_\alpha^{(3)} - \Sigma_\alpha^{(4)}\right), \tag{41}$$

$$\delta\Sigma_\alpha^{EW(d)} = i\pi\epsilon\left(\Sigma_\alpha^{(4)} - \Sigma_\alpha^{(5)}\right), \tag{42}$$

$$\delta\Sigma_\alpha^{EW(e)} = i\epsilon\cos(\pi/3)\left(\Sigma_\alpha^{(6)} - \Sigma_\alpha^{(4)}\right) = \frac{i\pi\epsilon}{2}\left(\Sigma_\alpha^{(6)} - \Sigma_\alpha^{(4)}\right), \tag{43}$$

$$\delta\Sigma_\alpha^{EW(f)} = i\pi\epsilon\cos(\pi/3)\left(\Sigma_\alpha^{(4)} - \Sigma_\alpha^{(7)}\right) = \frac{i\pi\epsilon}{2}\left(\Sigma_\alpha^{(4)} - \Sigma_\alpha^{(7)}\right), \tag{44}$$

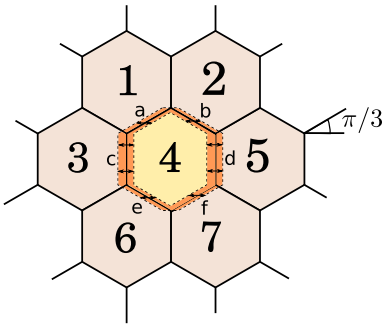

Fig. 3. Scheme of a hexagonal assembly vibrating in the x direction.

Table 1
Cross sections of the homogeneous material of the 1 D slab reactor.

g	D_g (cm)	Σ_{ag} (1/cm)	$\nu\Sigma_{fg}$ (1/cm)	Σ_{12} (1/cm)
1	1.40343	1.17659 e−2	5.62285 e−3	1.60795 e−2
2	0.32886	1.07186 e−1	5.90546 e−2	

Table 2
Kinetic data for the 1 D slab reactor.

β_{eff}	λ_{eff} (s^{-1})	$\mathbf{v}_1$ (cms^{-1})	$\mathbf{v}_2$ (cms^{-1})
0.0065	0.0767	1.8230 e+7	4.1306 e+5

where factor $\cos(\pi/3) = 1/2$ is introduced in faces a, b, e and f due to their inclination with the vibration direction (see Fig. 3). Note that, the spatial delta function is not taken into account because the integrals are taken along the edges, as Eq. (38) shows.

5. Application to case studies

5.1. One-dimensional slab reactor

The first and simplest studied case is a homogeneous one-dimensional slab reactor of longitude $2a = 300$ cm with zero flux boundary conditions. Table 1 shows values of the cross sections of each homogeneous material. The value of the mean number of neutrons produced by fission is assumed to be $\nu = 2.5$. The kinetic data of this problem are shown in Table 2. A point *generic absorber of variable strength* perturbation is situated at $x' = -30$ cm with a frequency of 1 Hz and a strength of $\delta\Sigma_{a1} = \Sigma_{a1}$ and $\delta\Sigma_{a2} = \Sigma_{a2}$. This problem has been solved analytically using the Green's functions technique exposed in Demazière (2011).

Fig. 4 shows the relative neutron noise amplitude obtained by using `FEMFFUSION`, `CORE SIM+` (Demazière, 2011; Mylonakis et al., 2021) and from the analytical solution. The `FEMFFUSION` calculation has used the edge-wise methodology inserting the perturbation at the interface situated at $x' = -30$ cm and The `CORE SIM+` computation has used an equidistant mesh of 60 cells of 5 cm each, where the point perturbation is inserted uniformly in the cell containing the point source. Fig. 5 displays the relative error of the neutron noise amplitude for the one-dimensional slab. The relative

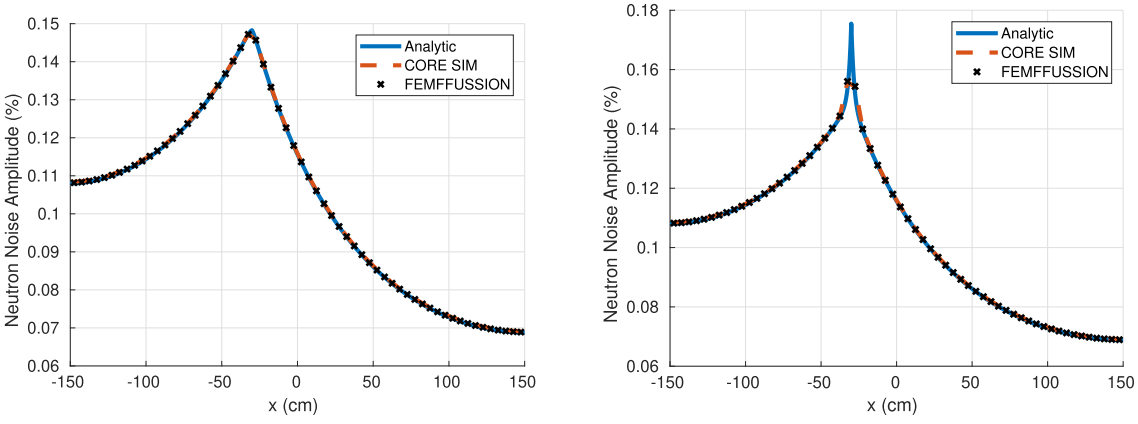

(a) Fast Flux Noise (b) Thermal Flux Noise

Fig. 4. Amplitude of the neutron noise for the one-dimensional slab.

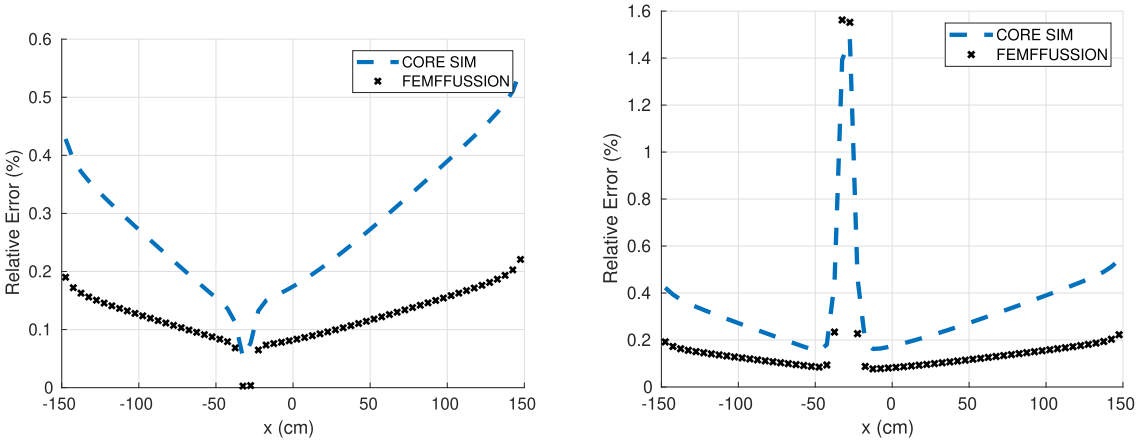

(a) Fast Flux Noise (b) Thermal Flux Noise

Fig. 5. Relative error of the neutron noise amplitude for the one-dimensional slab.

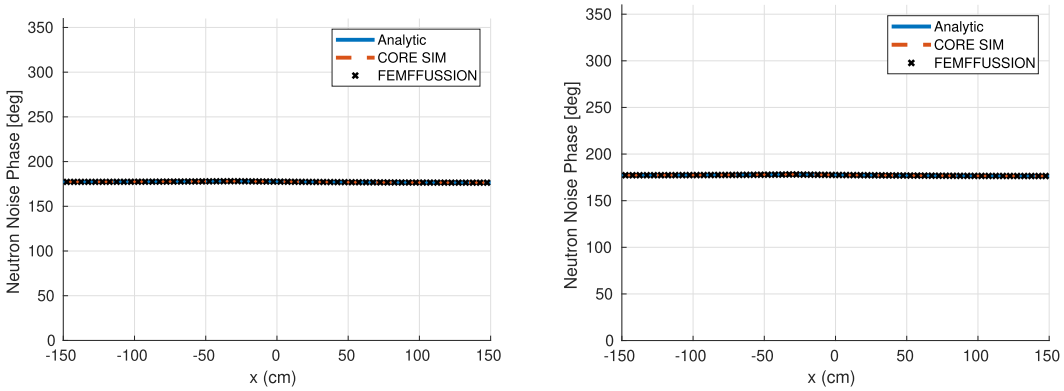

(a) Fast Flux Noise (b) Thermal Flux Noise

Fig. 6. Phase of the neutron noise for the one-dimensional slab.

maximum differences (RMD) between FEMFFUSION and the analytical solution are 0.22% and 1.56 % for fast and thermal neutron noise amplitudes, respectively. For CORE SIM+, the relative maximum errors are 0.54 % and 1.56%, respectively. The highest errors are located around the perturbation. Fig. 6 shows the phase of the neutron noise. A close agreement between the three strategies can be observed both on the neutron noise amplitude and on the neutron noise phase.

5.2. Two-dimensional rectangular case

Next, an example of a simple rectangular reactor with a moving assembly is presented. This example has 3×3 assemblies, where the central assembly is vibrating with a frequency of 1 Hz and an amplitude of 1 mm in the x direction, as Fig. 7 shows. The size of the reactor is 60×60 cm. Fig. 7 also displays the material configuration of the example. Table 7 shows the cross sections used for this case. In this case, it is also assumed that $\nu = 2.5$. The kinetic data for this problem are the same as the ones used in the previous problem, which are shown in Table 2.

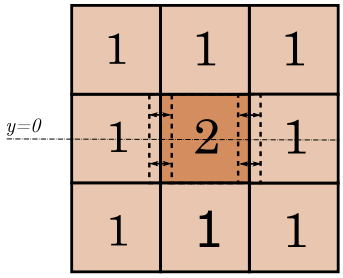

Fig. 7. Material distribution of the 2 D rectangular example.

Four different calculations have been compared in this example. First, a cell-wise frequency-domain calculation is performed with FEMFFUSION (Cell-wise FD). This calculation uses a 56×24 mesh, where four thin layers of cells of 1 mm are introduced to insert the perturbation source on the path of the moving assembly. Secondly, an edge-wise frequency-domain calculation is done with FEMFFUSION where the perturbation is introduced on the moving interface (Edge-wise FD calculation). This calculation uses a 24×24 equidistant mesh and provides accurate results without additional cells. Thirdly, as reference, a time-domain calculation is performed with the time-domain version of FEMFFUSION code. This code calculates the position of the vibrating assembly each time step and employs a volume homogenized cross section in the integration of the neutron diffusion equation. A refined mesh around the moving interfaces is used. Fourthly, a time-domain calculation performed with the time-dependent nodal code PARCS is studied. The same refined mesh is used for the time-dependent codes PARCS and FEMFFUSION and the frequency-domain cell-wise FD calculation.

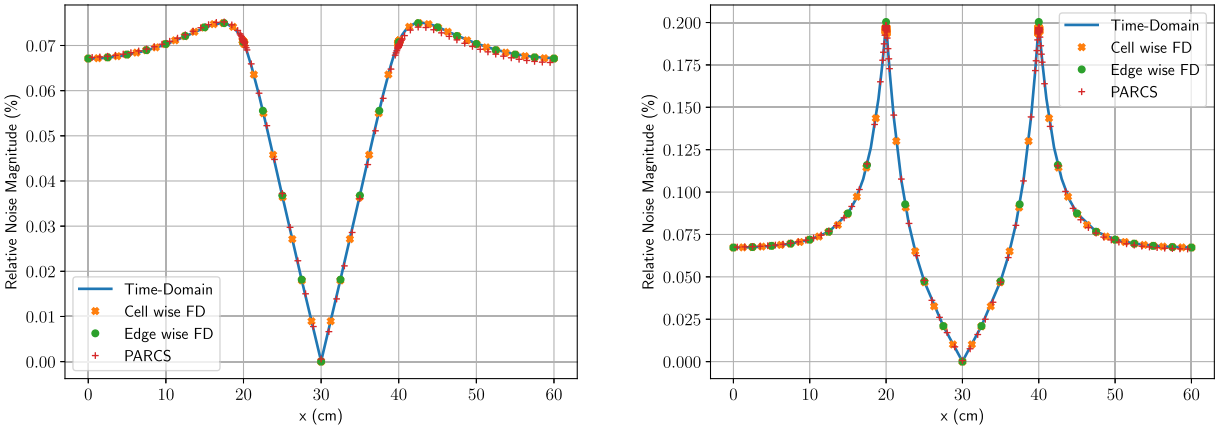

(a) Fast Flux Noise (b) Thermal Flux Noise

Fig. 8. Amplitude of the neutron noise for the 2 D rectangular example along the line $y = 0$ cm.

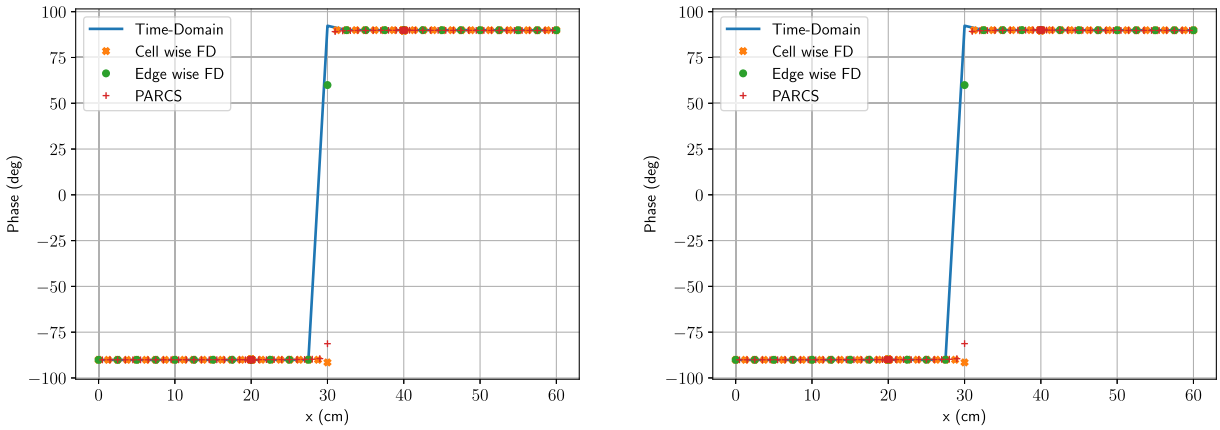

(a) Fast Flux Noise

(b) Thermal Flux Noise

Fig. 9. Phase of the neutron noise for the 2 D rectangular example along the line $y = 0$ cm.

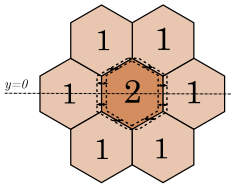

Fig. 10. Material distribution of the 2 D hexagonal example.

Fig. 8 shows a comparison of the relative neutron noise amplitude through the central line of the reactor ($y = 0$ cm) using these 4 strategies. Fig. 8 shows the neutron noise phase for this reactor example. Table 4 shows the Relative maximum difference (RMD) and relative average difference (RAD) of the magnitude of the neutron noise with respect to `FEMFFUSION` time-domain computation for the other 3 strategies. Only small differences among the four strategies, less than 4 %, can be observed around the moving interfaces of the vibrating assembly. In this way, the fastest calculation in terms of CPU time is to use the edge-wise FD calculation, which does not make use of a refined mesh near the perturbation, without loss of accuracy (see Fig. 9).

5.3. Two-dimensional hexagonal example

Here, an example of a simple hexagonal reactor with a moving assembly is presented. This example describes a 7 assemblies reactor, where the central assembly is vibrating with a frequency of 1 Hz and an amplitude of 1 mm in the x direction. The pitch of each hexagonal assembly is 15 cm. Fig. 10 displays the material configuration of this example. The cross sections and the kinetic data used are the same as in the previous example (Table 3 and Table 2, respectively).

In this case, three different calculations were performed. First, a frequency-domain edge-wise calculation is done. In this calculation, the perturbation source is inserted on the edges of the vibrating hexagonal assembly. As the assembly is moving in the x direction, the vertical edge has the double perturbation strength than the diagonal edges due to the fact that $\cos(\pi/3) = 1/2$. Second, as reference, two time-domain calculations were performed with `FEMFFUSION`. These calculations used a fixed mesh and volume averaged cross sections to represent the movement of the assembly each time-step, but with two different meshes, a uniform fixed mesh using 336 cells (called: TD N = 336) and a more refined uniform mesh using 2688 cells (called: TD N = 2688).

Fig. 11 shows the relative neutron noise amplitude in this simplified example computed with the edge-wise FD strategy

Table 3
Cross sections of the materials of the 2 D examples.

Material	Group	D_g (cm)	Σ_{ag} (1/cm)	$\nu\Sigma_{fg}$ (1/cm)	Σ_{12} (1/cm)
1	1	1.5000	0.000	0.000	2.000 e–02
	2	0.4000	8.000 e–02	1.350 e–01	
2	1	1.5000	0.000	0.000	2.000 e–02
	2	0.4000	8.500 e–02	1.350 e–01	

Table 4
Relative maximum difference (RMD) and relative average difference (RAD) of the magnitude of the neutron noise with respect to `FEMFFUSION` time-domain computation along the line $y = 0$ cm.

	Fast Group		Thermal Group	
	RMD (%)	RAD (%)	RMD (%)	RAD (%)
Cell-wise FD	0.47	0.16	0.76	0.25
Edge-wise FD	0.47	0.16	1.37	0.39
PARCS	3.89	1.24	3.41	1.05

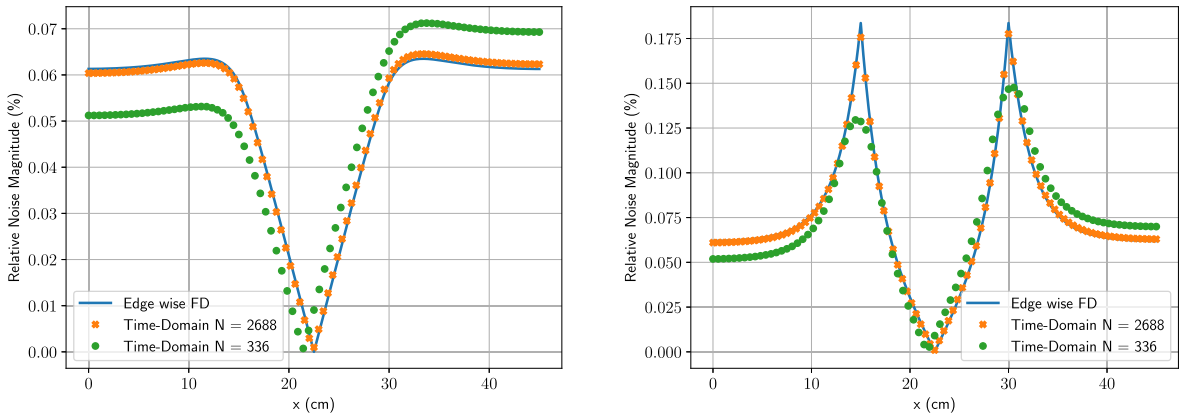

(a) Fast Flux Noise (b) Thermal Flux Noise

Fig. 11. Amplitude of the neutron noise for the 2 D hexagonal example along the $y = 0$ line.

Table 5
Relative maximum difference (RMD) and relative average difference (RAD) of the magnitude of the neutron noise with respect to `FEMFFUSION` edge-wise computation for the 2 D hexagonal example along the $y = 0$.

	Fast Group		Thermal Group	
	RMD (%)	RAD (%)	RMD (%)	RAD (%)
TD N = 336	231.06	23.54	173.26	18.32
TD N = 2688	24.95	2.80	18.26	2.11

and the time-domain computations over the midline of the reactor. Table 5 shows the RMD and RAD of the neutron noise amplitude. These results show that the time-domain computation with a coarse mesh (N = 336) does not represent accurately the neutron noise results, and it displays a non-physical non-symmetric behaviour. The coarse mesh shows an average difference of more than 18 %. On the other hand, the edge-wise frequency-domain strategy and the time-domain strategy with the fine mesh (N = 2688) show similar results, even though a small non-symmetry behaviour can be seen in the time-domain fine mesh calculation. Their relative average different is less than 3 %. The elevated relative maximum differences are around the centre of the reactor, where the noise amplitude is zero. Fig. 12 shows the neutron noise phase for this problem. The common discontinuous change of 180 degrees in the neutron noise phase around the perturbed assembly is observed (Vidal-Ferràndiz et al., 2020). Similar conclusions as the ones obtained for the noise amplitude are gathered for the noise phase computations, i.e. the time-domain computation with a coarse mesh does not represent accurately the phase results,

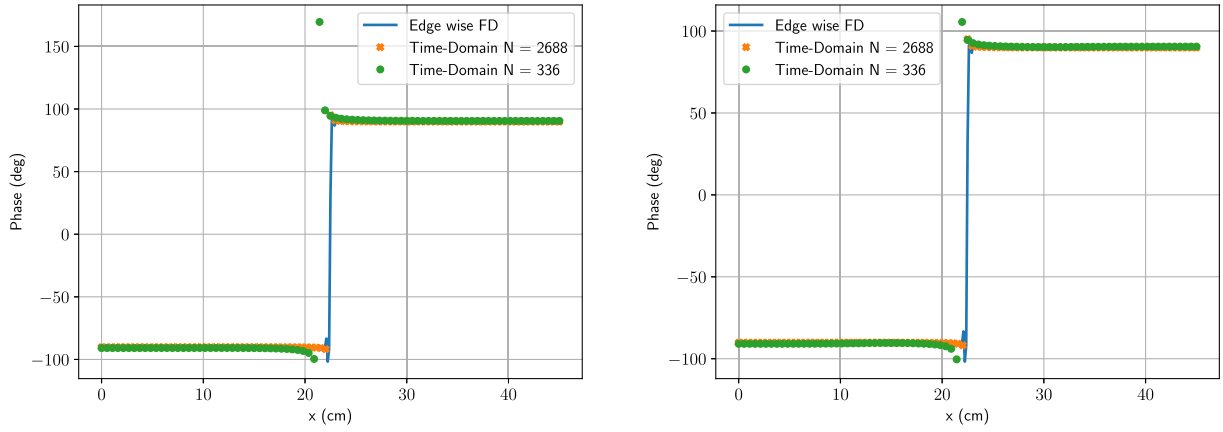

(a) Fast Flux Noise (b) Thermal Flux Noise

Fig. 12. Phase of the neutron noise for the 2 D hexagonal example along the $y = 0$ line.

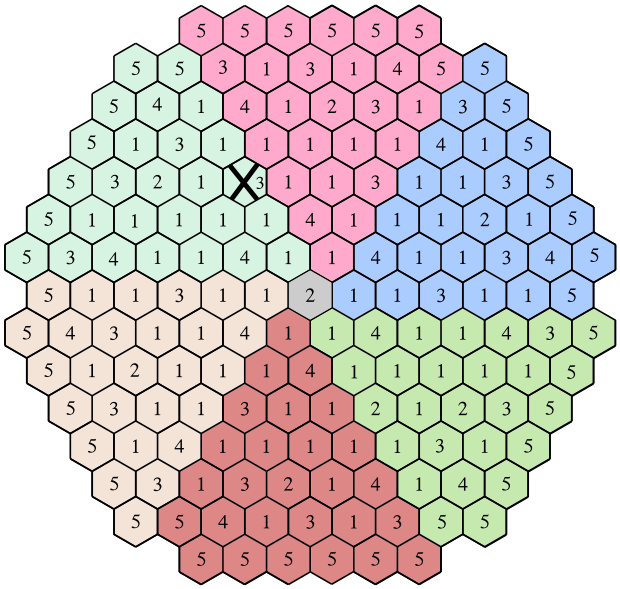

Fig. 13. Materials layout of the VVER-1000 reactor.

while the EW-FD strategy and the TD strategy with the fine mesh show similar results.

5.4. Two-dimensional VVER-1000

As a more realistic case of study, a two-dimensional version of a hexagonal VVER-1000 reactor core without reflector is considered (Chao and Shatilla, 1995). This reactor has a 1/6 cyclic symmetry, but as the inserted perturbation is not symmetrical, the whole reactor must be modelled. The assembly pitch is 23.6 cm. The core is composed of 163 fuel assemblies. Fig. 13 shows the materials' layout of the core. Vacuum boundary conditions are assumed for this problem. Table 6 shows the cross section data for this reactor. The kinetic data of this problem are assumed to be the same as the ones used in the previous problems, shown in Table 2.

A mechanical vibration is inserted in the fuel assembly marked with a cross ($\times$) in Fig. 13. The mechanical vibration has an amplitude of 1 mm and 1 Hz of frequency.

This problem is calculated with a frequency-domain and a time-domain methodology using second order polynomials in the finite element method and a globally refined grid with 48 cells per hexagon. The total number of cells is 62592. The obtained multiplicative factor for this problem is k_{eff}= 1.00645. Fig. 14 shows the static results in the VVER-1000 reactor computed with the edge-wise FD strategy. Fig. 15 shows the neutron noise amplitude for

Table 6
Cross section data for VVER-1000 reactor.

Material	Group	$\Sigma_{tr,g}$ (1/cm)	Σ_{ag} (1/cm)	$\nu\Sigma_{fg}$ (1/cm)	Σ_{fg} (1/cm)	Σ_{12} (1/cm)
1	1	2.409871 e–1	8.38590 e–3	4.81619 e–3	1.86139 e–3	1.64977 e–2
	2	8.629380 e–1	6.73049 e–2	8.46154 e–2	3.48111 e–2	
2	1	2.410237 e–1	1.15550 e–2	4.66953 e–3	1.81560 e–3	1.47315 e–2
	2	8.560110 e–1	8.10328 e–2	8.52264 e–2	3.50622 e–2	
3	1	2.389109 e–1	8.94430 e–3	6.04889 e–3	2.36371 e–3	1.56219 e–2
	2	8.630550 e–1	8.44801 e–2	1.19428 e–1	4.91322 e–2	
4	1	2.390411 e–1	1.19932 e–2	5.91507 e–3	2.31026 e–3	1.40185 e–2
	2	8.597200 e–1	9.89671 e–2	1.20497 e–1	4.95721 e–2	
5	1	2.389384 e–1	9.11600 e–3	6.40256 e–3	2.50773 e–3	1.54981 e–2
	2	8.669450 e–1	8.93878 e–2	1.29281 e–1	5.31856 e–2	

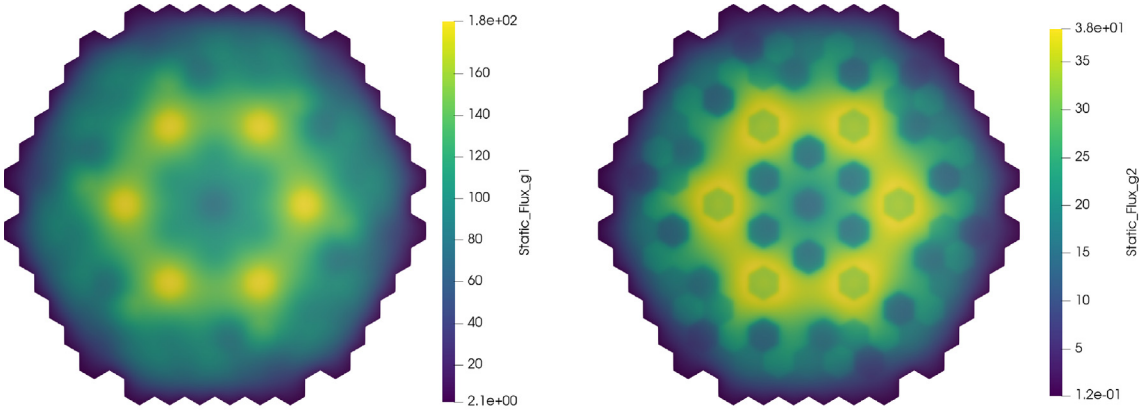

(a) Static Fast Flux

(b) Static Thermal Flux

Fig. 14. Static results for the VVER-1000 reactor.

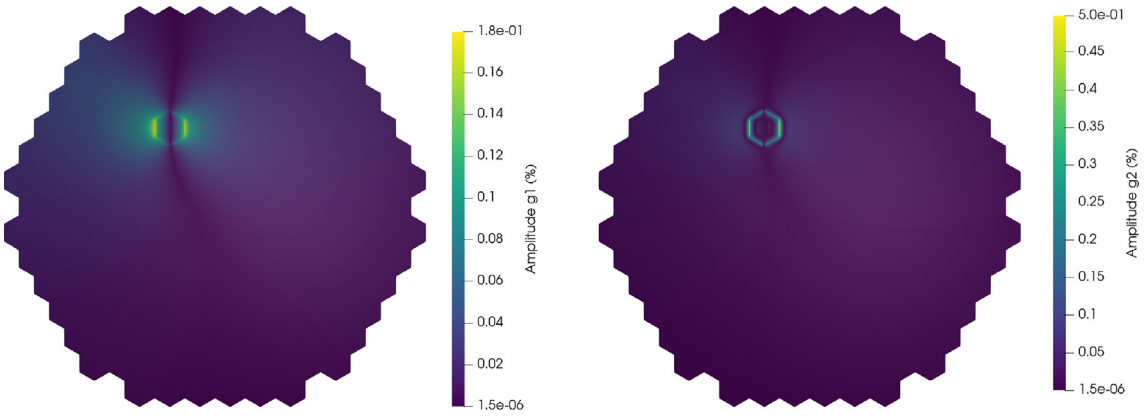

(a) Fast Noise (b) Thermal Noise

Fig. 15. Noise amplitude for the VVER-1000 reactor computed with the EW-FD strategy.

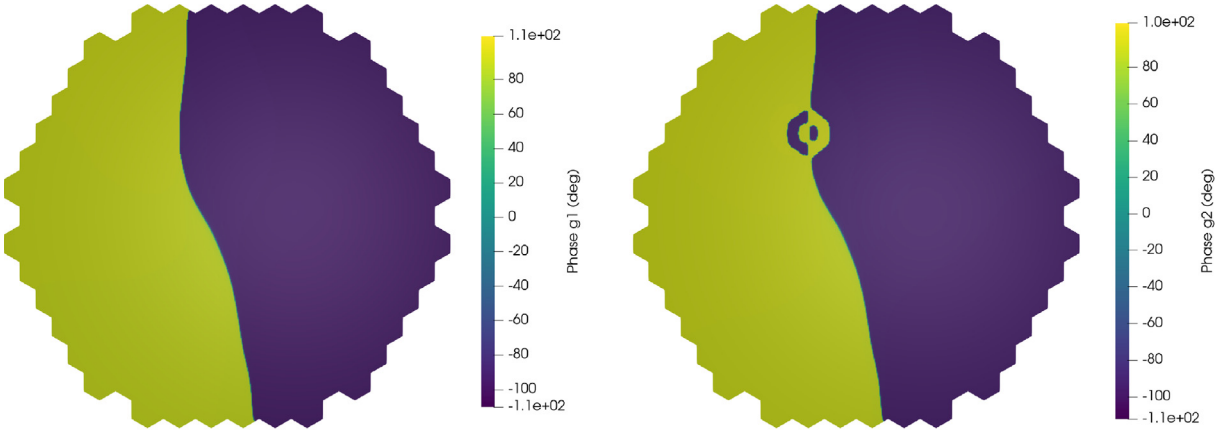

(a) Fast Noise (b) Thermal Noise

Fig. 16. Noise phase for the VVER-1000 reactor computed with the EW-FD strategy.

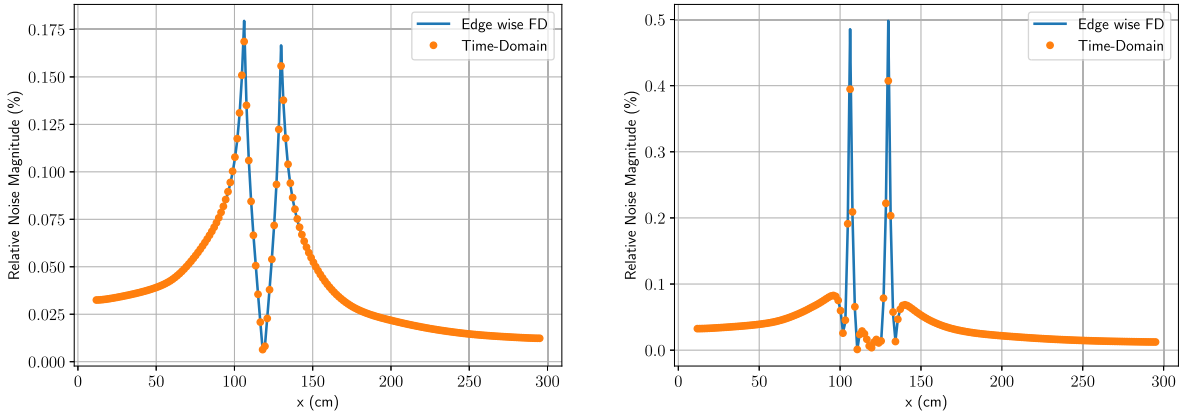

(a) Fast Flux Noise (b) Thermal Flux Noise

Fig. 17. Amplitude of the neutron noise for VVER-1000 reactor along the $y = 95.378$ cm line.

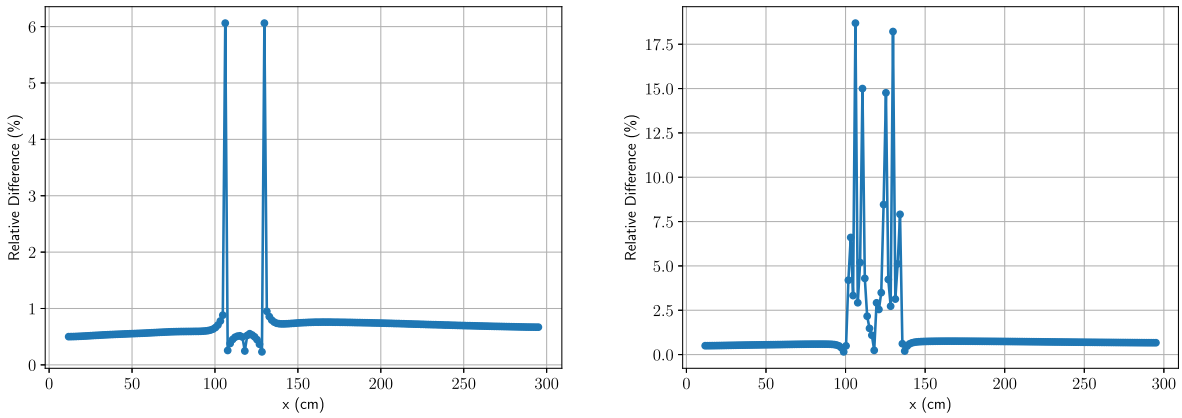

(a) Fast Flux Noise (b) Thermal Flux Noise

Fig. 18. Relative difference of the neutron noise amplitude between time-domain and edge-wise FD methodologies for the VVER-1000 reactor along the $y = 95.378$ cm line.

Table 7
Relative maximum difference (RMD) and relative average difference (RAD) for the VVER-1000 reactor along the $y = 95.378$ cm line.

	Fast Group		Thermal Group	
	RMD (%)	RAD (%)	RMD (%)	RAD (%)
Noise Amplitude	6.06	0.67	18.69	1.21
Noise Phase	2.26	0.31	5.06	0.38

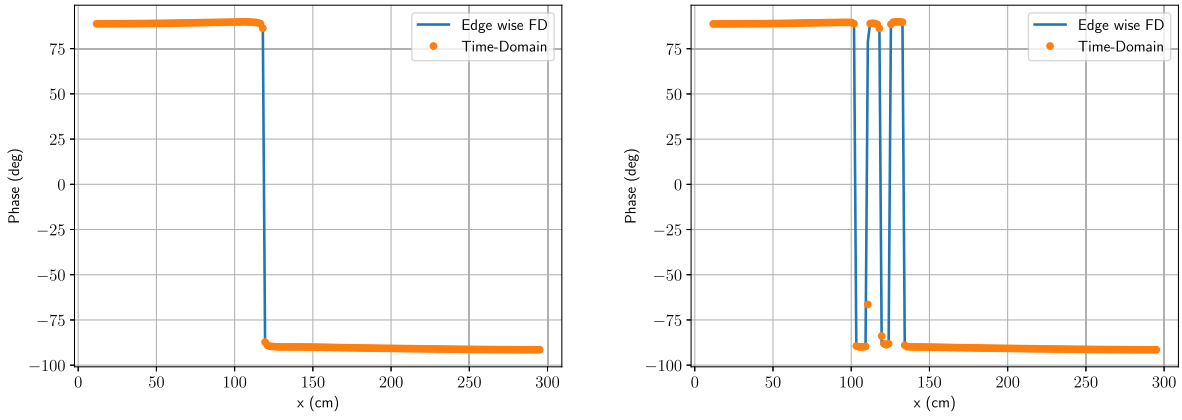

(a) Fast Flux Noise (b) Thermal Flux Noise

Fig. 19. Phase of the neutron noise for VVER-1000 reactor along the $y = 95.378$ cm line.

this problem. In this Figure, the neutron noise is concentrated in the boundaries of the vibrating assembly. The fast noise spreads over a larger region than the thermal neutron noise. Fig. 16 displays the noise phase for this problem. The usual change of 180 degrees in the neutron noise phase around the perturbed assembly is observed in the fast noise, and an additional change of phase can be observed inside the perturbed assembly. This fast change of phase cannot be accurately represented by the diffusion approximation because the transport effects grow with the gradient of the neutron flux.

Fig. 17 shows the relative neutron noise amplitude computed with the edge-wise FD strategy and the time-domain model. Fig. 18 displays the relative difference between the both methodologies, and Table 7 shows the RMD and the RAD for the VVER-1000 reactor along the $y = 95.378$ cm line. Edge-wise FD strategy and the time-domain model show similar results, the relative average differences are less than 1.3 %, and the maximum differences are located at the boundaries of the perturbed assembly. Fig. 19 shows the neutron noise phase for this problem. In the neutron noise phase, the agreement is closer because the relative average differences are about 0.4 %.

6. Conclusions

This work presents a neutron noise diffusion simulator in the frequency-domain developed using a high-order finite element method. It can deal with different kinds of reactor geometries and refinements. This code permits to introduce perturbations on the edges of the cells introducing the edgewise methodology and

allowing to model the mechanical vibrations of fuel assemblies accurately and efficiently, without using locally refined meshes around the perturbation. This feature is of special interest to simulate mechanical vibrations in non-rectangular geometries, as in hexagonal reactors.

Verification studies compare the frequency-domain simulations using the edge-wise methodology with the usual frequency-domain cell-wise model and the time-domain methodology. Small differences are shown in the results and this verifies the edge-wise model, showing that this methodology is efficient and can be implemented easily without the need to build ad hoc refined meshes near the perturbed assembly. This is an advantage because the size of the numerical problem to be solved is reduced and the generation of the mesh is simplified, especially in hexagonal geometries. In this way, the edge-wise methodology permits to simulate mechanical vibrations in three-dimensional hexagonal reactors without using complicated refined meshes. The edge-wise frequency-domain methodology has been also verified against other codes, as `CORE SIM+` and `PARCS` in rectangular reactors, obtaining results with good accuracy.

The limitations of the proposed strategy are concentrated in the use of the diffusion approximation because the neutron noise in the surroundings of the perturbed fuel assembly does not satisfy all the hypothesis needed to make valid the diffusion approximation. Future works will be devoted to study higher approximations of the neutron transport equation to model FA vibrations in the frequency-domain.

Declaration of Competing Interest

The authors declare that they have no known competing financial interests or personal relationships that could have appeared to influence the work reported in this paper.

Acknowledgements

This project has received funding from the Euratom research and training program 2014–2018 under grant agreement No 754316.

References

Balay, S., Abhyankar, S., Adams, M.F., Benson, S., Brown, J., Brune, P., Buschelman, K., Constantinescu, E.M., Dalcin, L., Dener, A., Eijkhout, V., Gropp, W.D., Hapla, V., Isaac, T., Jolivet, P., Karpeev, D., Kaushik, D., Knepley, M.G., Kong, F., Kruger, S., May, D.A., McInnes, L.C., Mills, R.T., Mitchell, L., Munson, T., Roman, J.E., Rupp, K., Sanan, P., Sarich, J., Smith, B.F., Zampini, S., Zhang, H., Zhang, H., Zhang, J., 2021. PETSc Web page. https://petsc.org/.

Bangerth, W., Hartmann, R., Kanschat, G., 2007. deal.II – a general purpose object oriented finite element library. ACM Trans. Math. Softw. 33 (4), 24/1–24/27.

Chao, Y.A., Shatilla, Y.A., 1995. Conformal mapping and hexagonal nodal methods - II: Implementation in the ANC-h code. Nucl. Sci. Eng. 121 (2), 210–225.

Demazière, C., 2011. CORE SIM: A multi-purpose neutronic tool for research and education. Ann. Nucl. Energy 38 (12), 2698–2718.

Demazière, C., Vinai, P., Hursin, M., Kollias, S., Herb, J., 2017. Noise-Based Core Monitoring and Diagnostics - Overview of the project. In: Advances in Reactor Physics (ARP-2017). Mumbai, India, pp. 1–4.

Gammicchia, A., Santandrea, S., Zmijarevic, I., Sanchez, R., Stankovski, Z., Dulla, S., Mosca, P., 2020. A MOC-based neutron kinetics model for noise analysis. Ann. Nucl. Energy 137, 107070.

Gong, H., Chen, Z., Wu, W., Peng, X., Li, Q., 2021. Neutron noise calculation: A comparative study between SP3 theory and diffusion theory. Ann. Nucl. Energy 156, 108184.

González-Pintor, S., Ginestar, D., Verdú, G., 2009. High order finite element method for the lambda modes problem on hexagonal geometry. Ann. Nucl. Energy 36 (9), 1450–1462.

Hosseini, S.A., Mohamadbeygi, S., 2021. Neutron noise simulator based on the boundary element method (BEM). Ann. Nucl. Energy 159, 108327.

Hosseini, S.A., Vosoughi, N., Vosoughi, J., 2018. Neutron noise simulation using ACNEM in the hexagonal geometry. Ann. Nucl. Energy 113, 246–255.

Jonsson, A., Tran, H.N., Dykin, V., Pázsit, I., 2012. Analytical investigation of the properties of the neutron noise induced by vibrating absorber and fuel rods. Kerntechnik 77 (5), 371–380.

Kolali, A., Vosoughi, J., Vosoughi, N., 2021. Development of SD-HACNEM neutron noise simulator based on high order nodal expansion method for rectangular geometry. Ann. Nucl. Energy 162, 108496.

Larsson, V., Demazière, C., 2009. Comparative study of 2-group and diffusion theories for the calculation of the neutron noise in 1d 2-region systems. Ann. Nucl. Energy 36 (10), 1574–1587.

Malmir, H., Vosoughi, N., 2015. Propagation noise calculations in VVER-type reactor core. Prog. Nucl. Energy 78, 10–18.

Mylonakis, A., Vinai, P., Demazière, C., 2021. CORE SIM+: A flexible diffusion-based solver for neutron noise simulations. Ann. Nucl. Energy 155, 108149.

Mylonakis, A.G., Vinai, P., Demazière, C., 2020. Numerical solution of two-energy-group neutron noise diffusion problems with fine spatial meshes. Ann. Nucl. Energy 140, 107093.

Pázsit, I., 1988. Control-rod models and vibration induced noise. Ann. Nucl. Energy 15 (7), 333–346.

Rouchon, A., Zoia, A., Sanchez, R., 2017. Apr. A new monte carlo method for neutron noise calculations in the frequency domain. Ann. Nucl. Energy 102, 465–475.

Stacey, W.M., 2007. Nuclear Reactor Physics. Wiley, Weinheim, Germany.

Verdú, G., Ginestar, D., Vidal, V., Muñoz-Cobo, J., 1994. 3D Lambda-modes of the neutron-diffusion equation. Ann. Nucl. Energy 21 (7), 405–421.

Vidal-Ferràndiz, A., Carreño, A., Ginestar, D., Verdú, G., 2021. FEMFFUSION a finite element method code for nuclear reactor modelling. https://www.femffusion.imm.upv.es, accessed: 2021-12-01.

Vidal-Ferràndiz, A., Carreño, A., Ginestar, D., Demazière, C., Verdú, G., 2020. Neutronic simulation of fuel assembly vibrations in a nuclear reactor. Nucl. Sci. Eng. 194 (11), 1067–1078.

Vidal-Ferràndiz, A., Carreño, A., Ginestar, D., Demazière, C., Verdú, G., 2020. A time and frequency domain analysis of the effect of vibrating fuel assemblies on the neutron noise. Ann. Nucl. Energy 137, 107076.

Vidal-Ferràndiz, A., Carreño, A., Ginestar, D., Verdú, G., 2019. A block arnoldi method for the SPN equations. Int. J. Computer Math., 1–22

Vidal-Ferràndiz, A., Carreño, A., Ginestar, D., Verdú, G., 2020. A block arnoldi method for the SPN equations. Int. J. Computer Math., 341–357

Vidal-Ferràndiz, A., Fayez, R., Ginestar, D., Verdú, G., 2014. Solution of the lambda modes problem of a nuclear power reactor using an h–p finite element method. Ann. Nucl. Energy 72, 338–349.

Vidal-Ferràndiz, A., Fayez, R., Ginestar, D., Verdú, G., 2016. Moving meshes to solve the time-dependent neutron diffusion equation in hexagonal geometry. J. Comput. Appl. Math. 291, 197–208.

Yamamoto, T., 2018. Implementation of a frequency-domain neutron noise analysis method in a production-level continuous energy monte carlo code: Verification and application in a BWR. Ann. Nucl. Energy 115, 494–501.

Yi, H., Vinai, P., Demazière, C., 2021. Acceleration of a 2-dimensional, 2-energy group neutron noise solver base on a discrete ordinates method in the frequency domain. EPJ Web of Conferences 247, 21005.

Zienkiewicz, O.C., Taylor, R.L., Zhu, J.Z., 2013. The Finite Element Method: Its Basis and Fundamentals. Butterworth-Heinemann, Oxford.

Zoia, A., Rouchon, A., Gasse, B., Demazière, C., Vinai, P., 2021. Analysis of the neutron noise induced by fuel assembly vibrations. Ann. Nucl. Energy 154, 108061.